Intense source of cold cesium atoms based on a two-dimensional magneto–optical trap with independent axial cooling and pushing*

Jia-Qiang Huang(黄家强)[1,3], Xue-Shu Yan(颜学术)[2,3], Chen-Fei Wu(吴晨菲)[1,3], Jian-Wei Zhang(张建伟)[2,3], and Li-Jun Wang(王力军)[1,2,3,†]

[1] *Department of Physics, Tsinghua University, Beijing* 100084, *China*
[2] *Department of Precision Instrument, Tsinghua University, Beijing* 100084, *China*
[3] *Joint Institute for Measurement Science (JMI), Tsinghua University, Beijing* 100084, *China*

(Received 16 December 2015; revised manuscript received 15 January 2016; published online 20 April 2016)

We report our studies on an intense source of cold cesium atoms based on a two-dimensional (2D) magneto–optical trap (MOT) with independent axial cooling and pushing. The new-designed source, proposed as 2D-HP MOT, uses hollow laser beams for axial cooling and a thin pushing laser beam to extract a cold atomic beam. With the independent pushing beam, the atomic flux can be substantially optimized. The total atomic flux maximum obtained in the 2D-HP MOT is 4.02×10^{10} atoms/s, increased by 60 percent compared to the traditional 2D$^+$ MOT in our experiment. Moreover, with the pushing power 10 μW and detuning 0Γ, the 2D-HP MOT can generate a rather intense atomic beam with the concomitant light shift suppressed by a factor of 20. The axial velocity distribution of the cold cesium beams centers at 6.8 m/s with an FMHW of about 2.8 m/s. The dependences of the atomic flux on the pushing power and detuning are studied in detail. The experimental results are in good agreement with the theoretical model.

Keywords: cold atomic beam, magneto–optical trap, light shift

PACS: 37.10.Gh, 37.20.+j, 37.10.De **DOI:** 10.1088/1674-1056/25/6/063701

1. Introduction

Cold atomic beams have desirable features such as high flux at low mean velocity, narrow velocity distribution, and small divergence. They are widely used in fields of atom interferometry,[1–4] atomic clocks,[5–8] cold atom collisions,[9,10] and atom optics.[11] Besides, they are required for fast loading a magneto–optical trap (MOT) in an ultra high vacuum (UHV).[12]

The cold atomic beams can be produced by using a Zeeman slower[13] or an isotropic-light tube[14] to decelerate a thermal atomic beam along its propagation axis, or by extracting from a vapor MOT directly. Compared to the decelerator, the MOT source is preferred because of its narrower velocity distribution and higher brightness.[15] The MOT source can be implemented in various configurations, including the low-velocity intense source (LVIS),[16–18] the moving molasses (MM) MOT,[19] the pure two-dimensional (2D) MOT,[20] and the 2D$^+$ MOT.[21]

The 2D$^+$ MOT source is a configuration in which the two-dimensional magneto–optical trap is complemented with axial laser beams. With larger cooling volume and the capability of cooling or pushing in the axial direction, the 2D$^+$ MOT can produce a higher atomic flux at a similar or even lesser power consumption than other configurations of the MOT source. For the axial laser beams, the configuration can be a pair of cooling beams (pushing and retarding beams),[21–24] one hollow beam,[25,26] or one pushing beam.[27–34] For the pair-of-beam configuration, the atoms are both cooled and pushed in the axial direction, which results in a high flux and a narrow axial-velocity distribution. Nevertheless, the laser power and detuning are mainly adapted to axial cooling rather than pushing. Considering the physical fact in the MOT, cooling decelerates atoms but pushing accelerates atoms. The pushing beam cannot be substantially optimized until its power and detuning is regulated independently. Besides, the axial laser light coming out along the cold atoms is rather intense, resulting in considerable light shift. For the one-hollow-beam configuration, the laser beam is far blue-detuned and shaped into a Laguerre–Gaussian donut mode. Cold atoms in the MOT can be channeled over a long distance with small divergence. Thus the atomic density is increased compared to that in a freely-propagating beam. In Carrat *et al.*'s recent study, the increase by a factor of 200 is achieved.[26] However, without axial cooling, the cold atoms from this kind of 2D$^+$ MOT have undesired broad axial velocity distribution, tens of meters per second. For the one-pushing-beam configuration, the pushing beam can be a thin near-resonant beam,[27–32] or an intense far-detuned one.[33,34] These studies, especially the 2D^{2p} MOT by Park *et al.*,[32] indicate that the pushing beam should have specific power and detuning. Though the pushing beam is optimized, without axial cooling, the efficiency of this kind of

*Project supported by the National Natural Science Foundation of China (Grant No. 11304177).
†Corresponding author. E-mail: lwan@tsinghua.edu.cn
© 2016 Chinese Physical Society and IOP Publishing Ltd

$2D^+$ MOT is lower than the first configuration.

In general, to obtain an intense cold atomic beam with narrow velocity distribution with the $2D^+$ MOT, the axial cooling and pushing is indispensable. Limited by the configurations above, the $2D^+$ MOT cannot be fully optimized. Besides, for experiments based on a cold atomic beam, such as atom interferometry and atomic clock, the problem of the light shift due to the pushing beam should also be resolved.[3,4] To substantially optimize the $2D^+$ MOT and significantly suppress the light shift, we propose a novel configuration for the axial laser beams. In the scheme, a pair of counter-propagating hollow laser beams are applied for axial molasses cooling. Another homocentric thin laser beam is used for pushing. The hollow beams and the pushing beam are functionally separated and do not interfere with each other. We propose "2D-HP MOT" to name this new scheme distinguishing it from the traditional $2D^+$ MOT, where H stands for the hollow cooling beams and P the thin pushing beam.

This paper is organized as follows. In Section 2, we explain the basic principle of the 2D-HP MOT, including the rate and trapping equation, the atomic flux analysis and the light shift effect. In Section 3, we present a detailed description of the experimental setup and the measurement of the cold atomic beam. The experimental results and discussions are arranged in Section 4. We summarize and give an outlook on future experiments in Section 5.

2. Principle of operation and theoretical model

The flux of the cold atomic beam extracted from the 2D-HP MOT is determined by the rate equation, the relationship between the loading rate and the loss rates. The loading rate R indicates the capture capability of the MOT, which is derived from the flux through the surface of the cooling volume of atoms with a radial velocity below the capture velocity $v_r < v_c$.[20,21,35] Its definition per axial velocity interval $[v_z, v_z + \mathrm{d}v_z]$ in cylindrical coordinate is[20]

$$R(n, v_z) = 2\pi r_c n \left(\frac{m}{2\pi k_B T}\right)^{3/2} \exp\left(-\frac{m v_z^2}{2k_B T}\right) \times \int_0^{v_c(v_z)} v_r \exp\left(-\frac{m v_r^2}{2k_B T}\right) 2\pi v_r \mathrm{d}v_r, \quad (1)$$

where r_c is the radius of the cooling volume, n the density of the thermal background vapor, m the atom mass, k_B the Boltzmann constant, and T the temperature of the vapor. According to Eq. (1), a high capture velocity results in a large loading rate. The capture velocity v_c depends on the axial velocity v_z. At low v_z, the cooling time is so long that the capture velocity can be simply regarded as a constant v_{c0}, which is around 30 m/s, and at high v_z, the capture velocity falls off as $1/v_z$.[20] In the 2D-HP MOT, the loading rate is optimized by applying the hollow laser beams to slow down atoms in the axial direction. With $v_c = 30$ m/s and $r_c = 8$ mm (see descriptions in Section 3), the total loading rate of the 2D-HP MOT over all the longitudinal velocity is approximately 5×10^{10} atoms/s.

The loss of the cold atoms within the MOT is mainly caused by three factors, which are the collisions between the cold atoms and the thermal background vapor ("cold–hot" collisions), the collisions between two cold atoms ("cold–cold" collisions), and the outcoupling from the cold atomic cloud into the beam, respectively. The loss rate due to the "cold–hot" collisions is proportional to the density of the thermal background vapor, which can be written as $\Gamma_{\mathrm{trap}} = n\sigma v_{\mathrm{rms}}$.[35] Here v_{rms} is the root-mean-square (rms) velocity of thermal atoms, and σ is the effective collision cross section. For a cesium atom, σ is 2×10^{-13} cm^2. The loss rate caused by the "cold–cold" collisions is $\beta_N N/V$, growing as the density of the trapped cold atoms. Here β_N is the trap-loss parameter, which contains the probabilities for inelastic processes, such as fine-structure-changing collisions, radiative escape, and photoassociation. The study on β_N has been an interesting and important topic. Both theoretical and experimental works verify that β_N increases linearly with the MOT laser intensity.[9,36,37] The loss rate due to the outcoupling is called the outcoupling rate Γ_{out}, which represents the capability of the pushing laser beam extracting the cold atomic beam from the MOT. It can be simply written as $\Gamma_{\mathrm{out}} = 1/t_{\mathrm{out}}$, where t_{out} is the time for pushing the cold atoms out of the MOT.[21]

In the 2D-HP MOT, the time t_{out} is determined by the cold atom velocity and the distance d that atoms travel out of the MOT. Under the radiation pressure from the pushing laser beam, the velocity is affected by the power and detuning and varies as

$$\frac{\mathrm{d}v_z(t)}{\mathrm{d}t} = \frac{\hbar k \Gamma}{2m} \frac{s}{1 + s + 4(\delta - \boldsymbol{k} \cdot \boldsymbol{v}_z(t))^2/\Gamma^2}, \quad (2)$$

where k is the wave vector, $\Gamma = 2\pi \cdot 5.22$ MHz the natural linewidth, $\delta = \omega_L - \omega_a$ the pushing laser detuning, and $s = I/I_s$ the saturation index. The velocity and t_{out} should meet the boundary condition

$$d = \int_0^{t_{\mathrm{out}}} v_z(t)\,\mathrm{d}t.$$

In this way, the outcoupling rate Γ_{out} can be calculated.

In addition to the three loss rates above, the heating effect due to the pushing laser beam also results in the loss of cold atoms. Obviously, this loss rate is related to the intensity and detuning of the pushing laser, and we assumed it can be expressed as $\Gamma_{\mathrm{heat}} \sim \alpha I \cdot s'$, where α is a coefficient, I is the pushing laser intensity, and $s' = s/(1 + s + 4(\delta - kv - \delta_{\mathrm{heat}})^2/\Gamma^2)$. The parameter δ_{heat} corresponds to the most effective heating detuning.

At the balance of loading and loss, the rate equation of the 2D-HP MOT can be written as[20,21]

$$R(n,v_z)-\Gamma_{\rm trap}N-\Gamma_{\rm out}N-\beta_N\frac{N^2}{V}-\Gamma_{\rm heat}N=0, \qquad (3)$$

where N is the cold atom number within the MOT. On the left side of Eq. (3), the third item, $\Gamma_{\rm out}N$, represents the cold atomic flux of a certain axial velocity. It can be expressed as

$$\Phi(n,v_z)=\Gamma_{\rm out}\left(\frac{-V(\Gamma_{\rm out}+\Gamma_{\rm trap}+\Gamma_{\rm heat})}{2\beta_N}+\frac{\sqrt{V^2(\Gamma_{\rm out}+\Gamma_{\rm trap}+\Gamma_{\rm heat})^2+4V\beta_N R(n,v_z)}}{2\beta_N}\right)\times\frac{v_z}{\Gamma_{\rm coll}}\left[1-\exp\left(\frac{\Gamma_{\rm coll}L}{v_z}\right)\right], \qquad (4)$$

where $\Gamma_{\rm coll}$ is the loss rate due to the light-assisted collisions between the atomic beam and the thermal vapor. The value of $\Gamma_{\rm coll}$ is proportional to the density of the background vapor, and usually one-order higher than $\Gamma_{\rm trap}$.[16] The total atomic flux of the 2D-HP MOT can be obtained by the integral Eq. (4) over all axial velocity $\Phi_{\rm tot}=\int_0^\infty\Phi(n,v_z)\,{\rm d}v_z$.

According to Eq. (4), the dependence of the total atomic flux on the outcoupling rate can be calculated. The results calculated with different loading rates, 5×10^{10} atoms/s, 1×10^{10} atoms/s, and 5×10^{9} atoms/s are as shown in Fig. 1. Here the other loss rates are treated as constant values. A high loading rate results in an intense flux and the total atomic flux increases with the outcoupling rate until saturated. Thus, to achieve an intense cold atomic beam, both the loading rate and the outcoupling rate should be adjusted to high values.

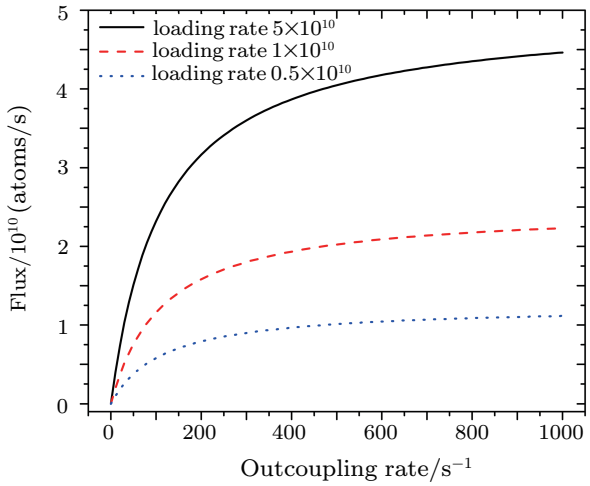


Fig. 1. (color online) The dependence of the total atomic flux on the outcoupling rate at different loading rates: 5×10^{10} atoms/s (black solid line), 1×10^{10} atoms/s (red dashed line), and 5×10^{9} atoms/s (blue dotted line).

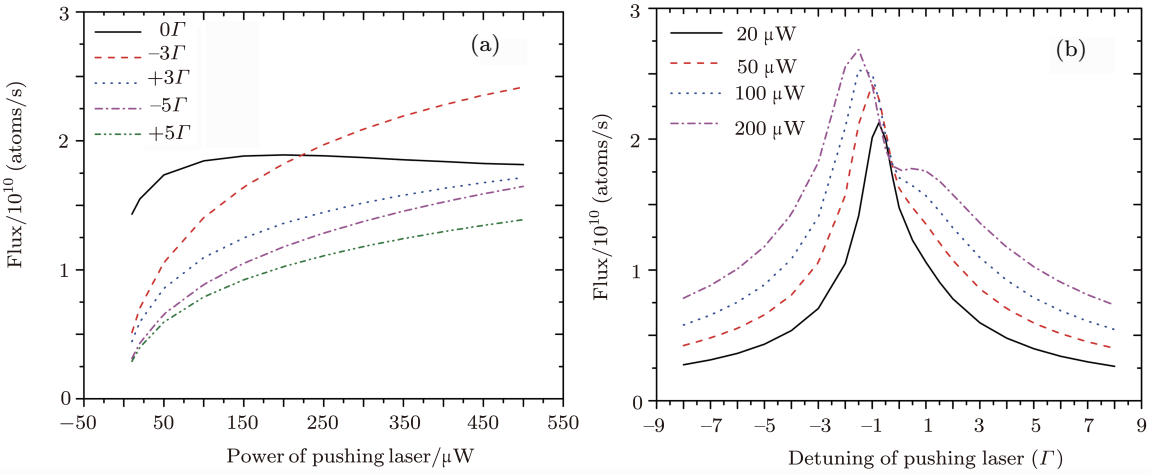


Fig. 2. (color online) The calculated atomic flux of the zero-velocity atoms: (a) the flux varying with the pushing power of various detunings, 0Γ (black solid line), -3Γ (red dashed line), $+3\Gamma$ (blue dotted line), -5Γ (magenta dashed-dotted line), and $+5\Gamma$ (green dash-dot-dot line); (b) the flux varying with the pushing detuning of various power, 20 μW (black solid line), 50 μW (red dashed line), 100 μW (blue dotted line), and 200 μW (magenta dashed-dotted line).

With trapping and sub-Doppler cooling, the velocity of the cold atoms in the MOT is close to zero value and follows a rather narrow Maxwell distribution.[21] Taking the average distance as $d=L/2=20$ mm and the initial axial velocity $v_z(0)=0$, the outcoupling rate $\Gamma_{\rm out}$ to different pushing power (beam diameter = 3 mm) and detuning can be calculated with Eq. (2) and the boundary condition. With the loading rate 5×10^{10} atoms/s, the dependences of the atomic flux on the pushing power and detuning are then obtained. In these results, the variations of the heating rate $\Gamma_{\rm heat}$ with the pushing laser parameters have been taken into calculations. As shown in Fig. 2(a), the atomic flux increases within a certain range of the pushing power. The resonant pushing beam generates the highest flux in low-power condition. But when the pushing power increases to a certain value, the atomic flux begins to decrease. This decrease is not found in the curves of the non-resonant conditions, because the pushing power is not enough. With the same detuning range, the red-detuned beam performs better than the blue-detuned one. In Fig. 2(b), we can find that the atomic flux decreases when the pushing laser detuning increases. As the pushing power grows, the laser frequency of the peak flux red-shifts, and the flux distribution broadens. In

high power conditions, the curve becomes much more asymmetric. These flux variations of the zero-velocity atoms provide a practical guidance for the pushing optimization in the 2D-HP MOT.

In addition to the independently-optimized atomic flux, the light shift is another main concern of the 2D-HP MOT. The light shift $\Delta\omega_F$ to the cesium atom is[38]

$$\Delta\omega_F = \frac{1}{4}\sum_{F'=F-1}^{F+1} |\Omega_{FF'}|^2 \frac{\delta_{FF'} - \boldsymbol{k}\cdot\boldsymbol{v}_z(t)}{(\delta_{FF'} - \boldsymbol{k}\cdot\boldsymbol{v}_z(t))^2 + \Gamma^2/4}, \quad (5)$$

where $\Omega_{FF'}$ is the Rabi frequency, $|\Omega_{FF'}|^2 = \Gamma^2 I/2I_s$ is proportional to the laser intensity, $\delta_{FF'} = \omega_L - \omega_{FF'}$ is the laser detuning, and $F = 3$ or 4 correspond to the ground states. In the 2D-HP MOT, atoms are slowed down by the hollow cooling beams. Thus, a near-resonant pushing beam with rather low power is enough to generate an intense atomic beam. By using a thin pushing beam, the light shift can be effectively suppressed. Moreover, the fluctuation of the light shift, which is much more destructive to signal contrast, can be significantly suppressed as the leaking light weakens.

3. Experimental setup and diagnostics

The experimental setup consists of the vacuum system, the quadrupole magnetic field, and the laser system. The cesium vapor cell is formed by a 55-mm diameter, long circular quartz tube. Both ends of the tube are connected to the pump system. Near the detection region, an ion pump is added to keep a higher vacuum. A temperature-controlled cesium reservoir is connected to the tube beside the MOT via a vacuum valve. In the experiments, the vacuum is 1.2×10^{-5} Pa at the MOT, and 3.5×10^{-6} Pa at the detection region.

The quadrupole magnetic field is generated by two orthogonal pairs of 140×100-mm rectangular coils, as shown in Fig. 3. The coils are spaced by 110 mm and symmetric in XY directions. Along the Z direction, it retains no magnetic field. The XY magnetic field gradient is set to be 10 Gs/cm (1 Gs $= 10^{-4}$ T).

The diode laser system includes a DBR laser, a DFB laser and an extended cavity diode laser (ECDL), which are all frequency-locked using the standard saturation absorption (SA) techniques. The DBR laser beam is split into two parts: one major part is used for the cooling and the other part is used as the pushing beam. The cooling frequency is detuned -2.5Γ from the cycling transition

$$6^2S_{1/2}(F=4) \rightarrow 6^2P_{3/2}(F'=5).$$

By means of two acoustic optical modulators (AOM), the pushing frequency can be shifted from -8Γ to 8Γ around the $4\rightarrow5'$ cycling transition. The DFB laser serves as the repumping laser and is frequency-locked to the transition

$$6^2S_{1/2}(F=3) \rightarrow 6^2P_{3/2}(F'=4).$$

The probe laser and the plug laser are derived from the ECDL laser beam and the plug laser is resonant with the $4\rightarrow5'$ cycling transition.

The configurations of the laser beams are presented in Fig. 3. To obtain a large cooling volume, the XY laser beams are expanded into 40 mm $\times$ 20 mm rectangles by the cylindrical lens. Containing 27-mW cooling laser and 4-mW repumping laser, the XY laser beams are circularly polarized and retro-reflected by $\lambda/4$ wave plates (50 mm $\times$ 25 mm). The $\lambda/4$ wave plates are coated with high-reflectivity film on the back to make the laser beams couterpropagate and polarize reversely. In this arrangement, the laser power requires higher values because of the imbalanced-laser effect.[15] In the axial direction, a hollow beam, which is linearly polarized and retro-reflected by another $\lambda/4$ wave plate, is applied for cooling as designed. The hollow beam is generated by an axicon, with the inner diameter 5 mm and the outer diameter 16 mm, and the power is 15 mW. At the center of the wave plate, a 1-mm aperture is drilled for atomic beam extraction. The pushing laser beam (beam diameter = 3 mm) is combined with the hollow beam by a polarized beam splitter (PBS). The pushing beam, the hollow beam and the aperture are aligned concentrically. In the experiment, a part of the pushing laser would leak out of the aperture and go along with the atomic beam. Here it is marked as "leaking laser light."

The plug laser and the probe laser are used for diagnosing the cold atomic beam. The plug laser is 2.5 mW with a 5-mm diameter, and the probe laser is a 200-μW rectangular beam (15 mm $\times$ 2 mm). The probe laser beam and plug laser beam are separated by 300 mm. To enhance the fluorescence signal, the probe laser beam is retro-reflected. The fluorescence emitted from the cold cesium atoms is collected by the lens assembly with a spatial angle Ω, and measured by a photodiode (Hamamatsu S3204-08). A time-of-flight (TOF) method is used to measure the atomic beam flux and the axial velocity distribution. Suddenly opening the plug beam, the cold atoms would be pushed away from the axis. The time dependence of the decaying fluorescence signal $S(\tau)$ is detected. Then the axial velocity distribution $\Phi(v_z)$ can be deduced as

$$\Phi(v_z) = -\frac{\eta}{d_{\text{probe}}}\frac{l}{v_z}\frac{\mathrm{d}S(\tau)}{\mathrm{d}\tau}, \quad (6)$$

where η is a calibration factor of the detection system, $d_{\text{probe}} =$ 2 mm is the width of the probe laser beam, and $l = 300$ mm is the distance between the plug laser and the probe laser. The total atomic flux in the experiments can be obtained by an overall integral of Eq. (6).

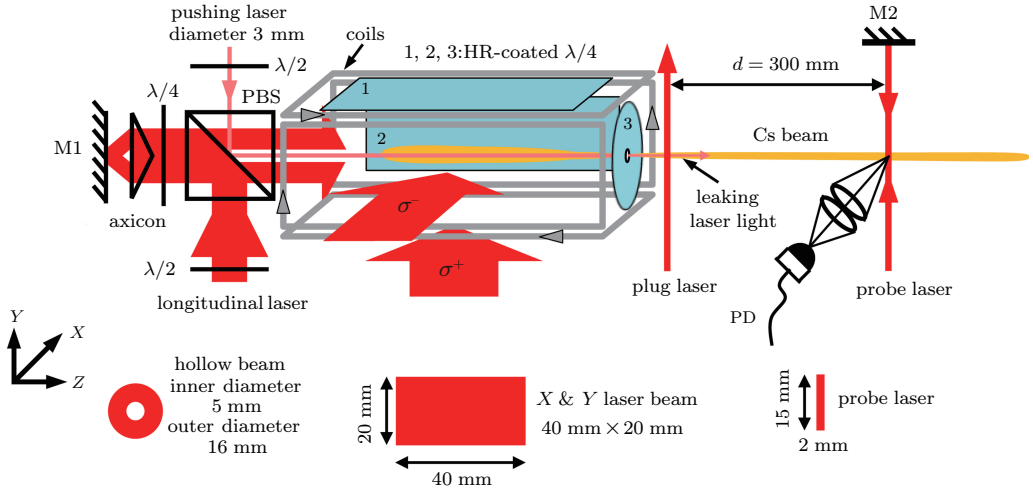


Fig. 3. (color online) The schematic diagram of the 2D-HP MOT. M_1, M_2: mirror; $\lambda/4$, $\lambda/2$: wave plate; PBS: polarized beam splitter; HR-coated $\lambda/4$: $\lambda/4$ wave plate coated with high-reflectivity film; σ^+, σ^-: circular polarization; Ω: collection angle; PD: photodiode.

4. Experimental results and discussion

In experiments, the 2D-HP MOT is realized, where the axial cooling and pushing are accomplished by a hollow beam and another pushing beam, respectively. The dependences of the total atomic flux on the pushing power and detuning are measured, and a comparison is made between the 2D-HP MOT and the traditional $2D^+$ MOT based on the experimental results.

4.1. Demonstration for the 2D-HP MOT

In the 2D-HP MOT, the hollow beam keeps the loading rate but makes no contribution to the atomic beam extraction, and the pushing beam regulating the outcoupling rate determines the atomic beam extraction. In experiment, the pushing beam is 15 μW and resonant with the $4 \rightarrow 5'$ cycling transition. By sweeping the probe laser frequency around the $4 \rightarrow 5'$ cycling transition, the hyperfine spectral lines of the cold atomic beam in different conditions are measured as shown in Fig. 4(a). When only the hollow beam is on, the cold cesium beam is not extracted, and the spectral line (blue dotted line) is almost invisible. When only the pushing beam is on, the spectral line (the red dashed line) is still very weak, because the loading rate is rather low without the axial cooling. When both the hollow and pushing beams are on, the spectral line (black solid line) becomes very distinct and the signal is enhanced by one order of magnitude of that in the only-pushing condition.

Besides, the axial velocity distribution in the pushing-only condition and the cooling-pushing condition is measured, as shown in Fig. 4(b). When only the pushing laser is on (red dashed line), the mean velocity of the distribution is 7.6 m/s and the total flux is 4.18×10^9 atoms/s. When both the cooling and pushing are on (black solid line), the mean velocity is reduced to 7.0 m/s, and the total flux is enhanced to 3.03×10^{10} atoms/s. The flux increases by about one order of magnitude, just as that of the spectral lines.

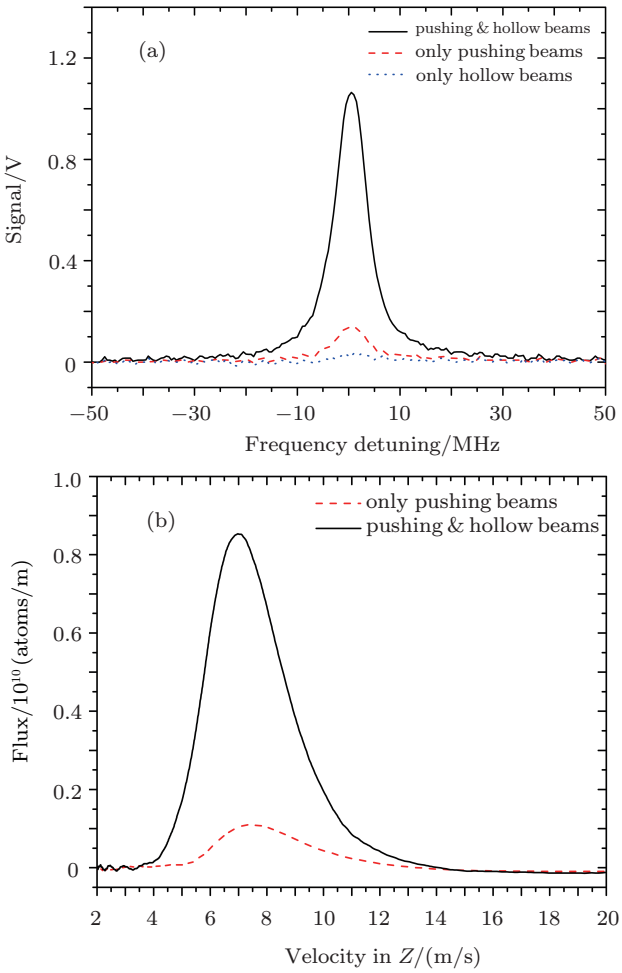


Fig. 4. (color online) Signal of the cold cesium atomic beam in different conditions: (a) the $4-5'$ hyperfine spectral lines: both hollow and pushing beams on (black solid line), only pushing beam on (red dashed line), only hollow beam on (blue dotted line); (b) the axial velocity distribution: only pushing beam on (red dashed line), both hollow and pushing beam on (black solid line).

These results demonstrate that the 2D-HP MOT works as

designed. The hollow beam keeps the loading rate and the pushing beam determines the outcoupling rate. An intense cold atomic beam is extracted when both laser beams are on.

4.2. Dependences on pushing parameters

In experiments, the dependence of the total atomic flux on the pushing power is measured at the detuning of -7Γ, -5Γ, 0Γ, $+5\Gamma$, and $+7\Gamma$, as shown in Fig. 5(a) and the results are the mean values of three measurements. The variations present that the total atomic flux would increase with the pushing power within a power range. This increase is caused by the enhanced outcoupling rate. At zero-detuning condition, a weak pushing power leads to a relatively high flux and the atomic flux reaches 3.03×10^{10} atoms/s, when the power is only 15 μW. After that, the atomic flux begins to decrease. The atomic flux at red detuning is higher than that at blue detuning. The maximum flux in experiments, 4.02×10^{10} atoms/s, is obtained when the pushing power is 400 μW and the detuning is at -5Γ. These results are in agreement with the theoretical calculation in Fig. 2(a).

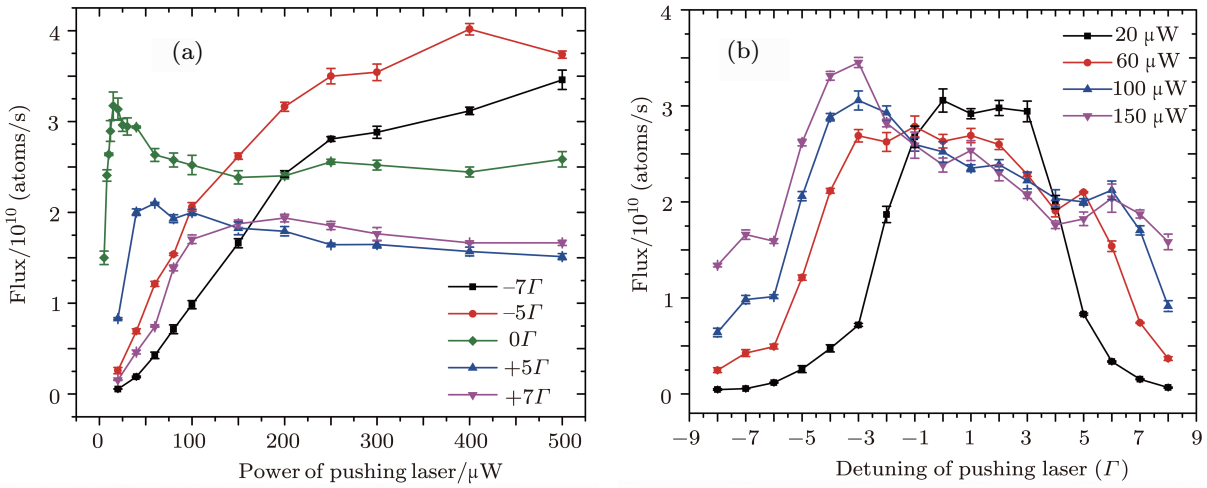


Fig. 5. (color online) The dependences of the total atomic flux on the pushing parameters: (a) the dependence on the pushing power at different pushing detuning: -7Γ (black square line), -5Γ (red circle line), 0Γ (green diamond line), $+5\Gamma$ (blue up triangle line), and $+7\Gamma$ (magenta down triangle line); (b) the dependence on the pushing detuning at different pushing power: 20 μW (black square line), 60 μW (red circle line), 100 μW (blue up triangle line), and 150 μW (magenta down triangle line).

Besides the 0Γ condition, the experimental results of $+5\Gamma$ and $+7\Gamma$ in Fig. 5(a) also show a clear decrease. The turning point of laser power has the minimum value at zero-detuning condition, and increases as the pushing detuning extends.

As discussed in Section 2, the heating effect caused by the pushing laser around the axis accounts for the flux loss. The heated atoms will escape from the MOT, rather than being pushed out, if its velocity is faster than the capture velocity. In experiments, the section of the pushing laser beam is a little larger than the aperture, which can generate a more serious heating effect when the pushing laser is suitably blue-detuned.

Additionally, the dependence of the total atomic flux on the pushing detuning at pushing power of 20 μW, 60 μW, 100 μW, and 150 μW are measured as shown in Fig. 5(b). When the power is as low as 20 μW, we can find that the total atomic flux has a higher value when the frequency of the pushing laser is close to resonance. With the pushing power increasing, the laser frequency corresponding to the peak flux red-shifts, and the high-flux range broadens. Besides, as the pushing power increases, the atomic flux near resonance decreases, instead of increasing as the outcoupling rate. These variations are consistent with the theoretical calculations in Fig. 2(b). Besides, it should be mentioned that the results in Fig. 2(b) are calculated with a zero axial velocity. The narrow Maxwell distribution of the cold atoms trapped in the MOT is not included. Thus, the variations of the flux with detuning in experiment is more broadened than that in theory. To fully reflect the reality, the velocity distribution of the cold atoms inside the MOT should be measured. However, limited by the experimental setup, a time-of-flight (TOF) measure around the MOT was not carried out in our experiments.

4.3. Comparison with the 2D$^+$ MOT

To compare to the traditional 2D$^+$ MOT with a pair of cooling beams, the 2D-HP MOT is modified by blocking the pushing beam and replacing the hollow laser beam by a regular Gaussian beam. The laser beam has the same diameter, power, and detuning as the previous hollow beam. The central intensity of the Gaussian beam is the pushing intensity, 8.06 mW/cm^2. Other parts of the setup in Fig. 3 remain unchanged. Thus, except the fixed pushing, other parameters of the 2D$^+$ MOT are the same as the 2D-HP MOT.

The axial velocity distribution of the cold atomic beam extracted from the 2D$^+$ MOT centers at 7.2 m/s with an FWHM of 3.2 m/s, the black solid line shown in Fig. 6(a).

The total atomic flux is 2.54×10^{10} atoms/s.

To make a comparison with the $2D^+$ MOT, the velocity distributions obtained in the 2D-HP MOT with the pushing parameters (-5Γ, 400 μW) and (0Γ, 10 μW) are plotted in Fig. 6(a). For the parameters -5Γ and 400 μW, the pushing laser intensity is 5.66 mW/cm^2. In this condition, the total atomic flux reaches the experimental maximum, 4.02×10^{10}. The velocity distribution centers at 8.2 m/s with an FWHM of 4.2 m/s (the blue dotted line in Fig. 6(a)). Compared to the $2D^+$ MOT, the total atomic flux is enhanced by 60%.

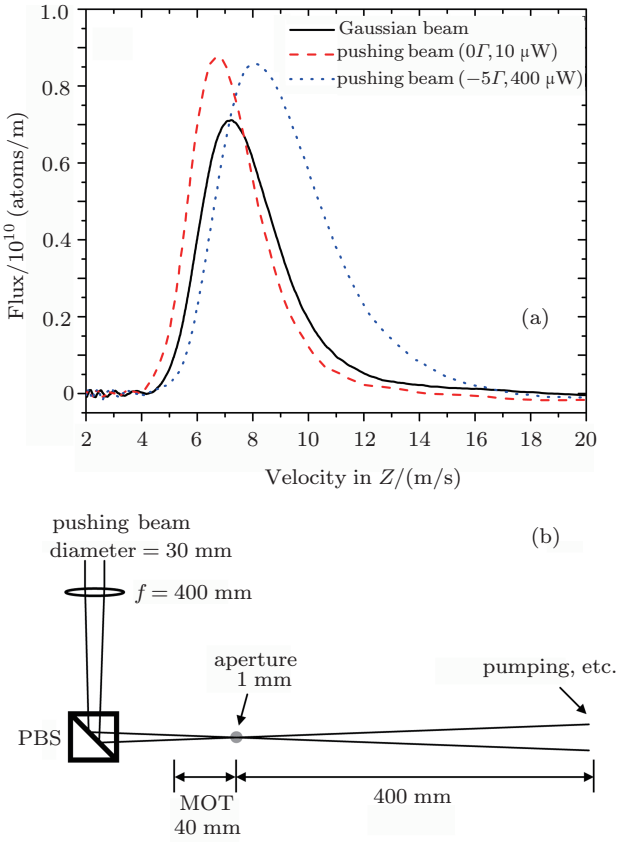


Fig. 6. (color online) (a) The axial velocity distributions of the cold atomic beams: $2D^+$ MOT (regular Gaussian beam, black solid line), 2D-HP MOT (0Γ, 10 μW, red dashed line), and 2D-HP MOT (-5Γ, 400 μW, blue dotted line). (b) Schematic diagram of the pushing beam expander.

For the parameters (0Γ, 10 μW), the pushing laser intensity is 0.14 mW/cm^2. In this condition, the velocity distributes around 6.8 m/s with an FWHM of 2.8 m/s (the red dashed line shown in Fig. 6(a)). The atomic flux is 2.64×10^{10} atoms/s, similar to the $2D^+$ MOT. However, the 0.14-mW/cm^2 pushing beam is much weaker than that of the $2D^+$ MOT, helping effectively suppress the light shift caused by the leaking laser light. According to Eq. (5), the light shift of the ground state hyperfine transition between $6^2S_{1/2}(F=3)$ and $6^2S_{1/2}(F=4)$ caused by the thin pushing laser is about -19.76 kHz, which is about 20 times lower than the one, -436.82 kHz, caused by the Gaussian beam. Moreover, with the same laser power instability, the light shift fluctuation is also drastically reduced. This suppression can greatly improve the signal in atomic clocks or atom interferometers.

Furthermore, with a minor adjustment to the thin pushing beam like those in Refs. [26] and [29], the light shift can be further suppressed. As shown in Fig. 6(b), the MOT axial length is 40 mm, and the region for experiments (pumping, probing, etc.) is 400 mm away from the beam-extraction aperture. By adjusting the pushing-beam diameter to 30 mm and placing a lens ($f = 400$ mm) 400 mm before the aperture, the beam diameter within the MOT region would be still as small as the one (3 mm) in Fig. 3. With the power 10 μW, the pushing laser intensity within the MOT would be almost unchanged. Thus, the pushing rate and the atomic flux are not affected. However, according to the law of geometrical optics, the leaking laser intensity in the experimental region would be reduced to about 1.4 μW/cm^2. Consequently, the light shift can be further decreased to about -200 Hz, about 100 times smaller than the value -19.76 kHz above. With the pushing power fluctuation suppressed by -50 dB,[39] the relative frequency uncertainty of an atomic clock based on this 2D-HP beam due to the light shift would be around 1×10^{-13}.

5. Conclusion and outlook

In this work, we present a new design for a source of cold cesium atoms, the 2D-HP MOT. With independent axial cooling and pushing, the 2D-HP MOT can substantially optimize the atomic flux. The atomic flux maximum obtained in the 2D-HP MOT is 4.02×10^{10} atoms/s, 60% higher than the traditional $2D^+$ MOT. With proper pushing parameters, the 2D-HP MOT can generate a rather intense cold atomic beam with the concomitant light shift 20 times smaller than that in the traditional $2D^+$ MOT. Compared to the traditional $2D^+$ MOT, the 2D-HP MOT needs some more facilities to provide the hollow beam and the pushing beam. But with the total atomic flux increased and the light shift suppressed, it can help improve the precision measurement experiments on cold atomic beams, for example, an atomic clock based on a continuous cold cesium atomic beam.

Acknowledgments

The authors especially acknowledge Lu Zhao, Chi Xu, Wei Xiong and Yu-Hang Li for their helpful discussions.

References

[1] Fixer J B, Foster G T, McGuirk J M and Kasevich M A 2007 *Science* **315** 74
[2] Muller H, Peters A and Chu S 2010 *Nature* **463** 926
[3] Xue H B, Feng Y Y, Chen S, Wang X J, Yan X S, Jiang Z K and Zhou Z Y 2015 *J. Appl. Phys.* **117** 094901
[4] Müler H, Chiow S W, Long Q, Herrmann S and Chu S 2008 *Phys. Rev. Lett.* **100** 180405

[5] Gibble K and Chu S 1993 *Phys. Rev. Lett.* **70** 1771

[6] Devenoges L, Stefanov A, Joyet A, Thomann P and Di Domenico G 2012 *IEEE Trans. Ultrason. Ferroelectr. Freq. Control* **59** 211

[7] Wang H and Iyanu G *P*roceedings of the IEEE International Frequency Control Symposium, June 2–4, 2010, California, USA, p. 454

[8] Vanier J 2005 *Appl. Phys. B* **81** 421

[9] Wanier J, Bagnato V S, Zilio S and Julienne P S 1999 *Rev. Mod. Phys.* **7** 1

[10] Zhao B S, Schewe H C, Meijer G and Schöllkopf W 2010 *Phys. Rev. Lett.* **105** 133203

[11] Adams C, Sigel M and Mlynek J 1994 *Phys. Rep.* **240** 143

[12] Donley E, Heavner T and Jefferts S 2005 *IEEE Trans. Instrum. Meas.* **54** 1905

[13] Lison F, Schuh P, Haubrich D and Meschede D 1999 *Phys. Rev. A* **61** 2483

[14] Ketterle W, Martin A, Joffe M A and Pritchard D E 1992 *Phys. Rev. Lett.* **69** 2483

[15] Ovchinnikov Y B 2005 *Opt. Commun.* **249** 473

[16] Lu Z T, Corwin K L, Renn M J, Anderson M H, Cornell E A and Wieman C E 1996 *Phys. Rev. Lett.* **77** 3331

[17] Feng Y Y, Zhu C X, Wang X J, Xue H B, Ye X Y and Zhou Z Y 2009 *Chin. Phys. B* **18** 3373

[18] Wang X J, Feng Y Y, Xue H B, Zhou Z Y and Zhang W D 2011 *Chin. Phys. B* **20** 126701

[19] Berthoud P, Fretel E and Thomann P 1999 *Phys. Rev. A* **60** R4241

[20] Schoser J, Batär A, Löw R, Schweikhard V, Grabowski A, Ovchinnekov Y B and Pfau T 2002 *Phys. Rev. A* **66** 023410

[21] Dieckmann K, Spreeuw R J C, Weidemülle and Walraven J T M 1998 *Phys. Rev. A* **58** 3891

[22] Wang H and Buell W F 2003 *J. Opt. Soc. Am. B* **20** 2025

[23] Chaudhuri S, Roy S and Unnikrishnan C S 2006 *Phys. Rev. A* **74** 023406

[24] Fang J C, Lu Q, Zhang Y C, Wang T Y, Li H R, Hu Z H and Quan W 2015 *J. Opt. Soc. Am. B* **32** B61

[25] Pruvost L, Marescaux D, Houde O and Duong H T 1999 *Opt. Commun.* **166** 199

[26] Carrat V, Cabrera-Gutierrez C, Jacquey M, Tabosa J W, de Lesegno B V and Pruvost L 2014 *Opt. Lett.* **39** 719

[27] Wohlleben W, Chevy F, Madison and Dalibard J 2001 *Eur. Phys. J. D* **15** 237

[28] Cacciapuoti L, Castrillo A, de Angelis M and Tino G M 2001 *Eur. Phys. J. D* **15** 245

[29] Catani J, Maioli L, de Sarlo L, Minardi F and Inguscio M 2006 *Phys. Rev. A* **73** 033415

[30] Castagna N, Guna J, Plimmer M D and Thomann P 2006 *Eur. Phys. J.: Appl. Phys.* **34** 21

[31] Wang J M, Wang J, Yan S B, Geng T and Zhang T C 2008 *Rev. Sci. Instrum.* **79** 123116

[32] Park S J, Noh J and Mun J 2012 *Opt. Commun.* **285** 3950

[33] Dimova E, Morizot O, Stern G, Alzar Garrido C L, Fioretti A, Lorent V, Comparat D, Perrin H and Pillet P 2007 *Eur. Phys. J. D* **42** 299

[34] Li K, Wang X R, He L X, Zhan M S and Lu B L 2007 *Chin. Phys. Lett.* **24** 2562

[35] Monroe C, Swann W, Robinson H and Wieman C 1990 *Phys. Rev. Lett.* **65** 1571

[36] Anwar M, Faisal M and Ahmed M 2013 *Eur. Phys. J. D* **67** 270

[37] Gallagher A and Pritchard D E 1989 *Phys. Rev. Lett.* **63** 957

[38] Affolderbach C, Andreeva C, Cartaleva S, Karaulanov T, Mileti G and Slavov D 2005 *Appl. Phys. B* **80** 841

[39] Kwee P, Willker B and Danzmann K 2011 *Appl. Phys. B* **102** 515